Nationaal Lucht- en Ruimtevaartlaboratorium
National Aerospace Laboratory NLR

Executive Summary

Destabilizing free shear layers in X-LES using a stochastic subgrid-scale model

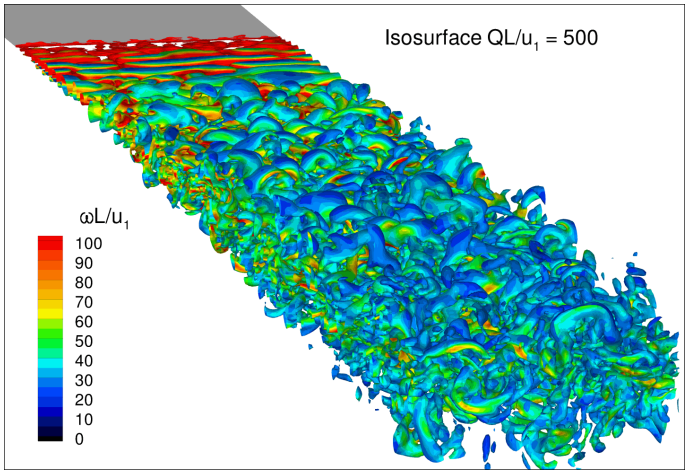

Problem area
Massively separated flows play an important role in topics such as the design of silent landing gear, the study of stability and control properties of fighter aircraft in relation to vortex breakdown, and the study of aerodynamic loads on structural aircraft components due to buffetting. These flows are strongly turbulent, involving a large range of spatial and temporal scales, which makes it difficult to model their dynamics with high physical accuracy and reliability. Flow computations based on the Reynold-averaged Navier–Stokes (RANS) equations are not able to capture the smaller turbulent scales. Large-eddy simulations (LES), on the other hand, do capture a significant range of scales, but are computationally too demanding for complex geometries. In recent years, therefore, research has focussed on hybrid RANS-LES methods, improving the physical accuracy compared to RANS, but without the cost of a full LES. In particular, NLR has developed the eXtra-Large Eddy Simulation (X-LES) method.

Description of work
An important issue in hybrid RANS–LES methods is the capturing of free shear layers. Typically, free shear layers are present between the attached boundary layers (computed with RANS) and the separated flow regions (computed with LES). These shear layers may develop too slowly in X-LES and similar hybrid RANS–LES meth-

Report no.
NLR-TP-2009-327

Author(s)
J.C. Kok and H. van der Ven

Classification report
Unclassified

Date
June 2009

Knowledge area(s)
Computational Physics &
Theoretical Aerodynamics

Descriptor(s)
Hybrid RANS-LES
Free shear layer
Sub-grid scale model

This report is based on a presentation held at the Third Symposium on Hybrid RANS–LES Methods, Gdansk, Poland, 10–12 June 2009.

ods. As a consequence the size of the separated flow regions may be overpredicted. Apparently, the computations are too clean compared to windtunnel or free-flight experiments: the shear layer remains stable, because there are no disturbances present that may trigger unstable modes. To resolve this issue, a stochastic term is introduced in the LES model.

Results and conclusions

For standard X-LES computations, the instabilities in a plane free shear layer develop very slowly and remain purely two dimensional. The plane shear layer is successfully destabilized by introducing a stochastic term in the LES model. Three dimensional instabilities develop rapidly and lead to fully developed, realistic turbulence within a short distance.

Applicability

Free shear layers appear in many applications, for example, vortical flows around fighter aircraft or landing gear wakes, and strongly influence the downstream flow development. For all these applications, the new stochastic method is relevant and may improve the computational results.

Nationaal Lucht- en Ruimtevaartlaboratorium, National Aerospace Laboratory NLR

Anthony Fokkerweg 2, 1059 CM Amsterdam,
P.O. Box 90502, 1006 BM Amsterdam, The Netherlands
Telephone +31 20 511 31 13, Fax +31 20 511 32 10, Web site: www.nlr.nl

Nationaal Lucht- en Ruimtevaartlaboratorium
National Aerospace Laboratory NLR

NLR-TP-2009-327

Destabilizing free shear layers in X-LES using a stochastic subgrid-scale model

J.C. Kok and H. van der Ven

This report is based on a presentation held at the Third Symposium on Hybrid RANS-LES Methods, Gdansk, Poland, 10-12 June 2009.

This publication has been refereed by the Advisory Committee AEROSPACE VEHICLES.

Customer	NLR
Contract number	----
Owner	NLR
Division NLR	Aerospace Vehicles
Distribution	Unlimited
Classification of title	Unclassified
	December 2009

Approved by:

Author	Reviewer	Managing department
18/12/09	2009/12/18	18-12-2009

Summary

In this paper, a stochastic term is introduced in the subgrid-scale model of the X-LES method in order to improve the computation of turbulent free shear layers. These shear layers may develop too slowly in X-LES and similar DES-type methods, even when fine grids and high-order numerical methods are used. For a plane free shear layer, the stochastic subgrid-scale model induces rapid development of fully 3D turbulence in contrast to the standard method for which the flow remains purely 2D. A comparison is made with experimental results and with results of a zonal RANS–LES method with LES content added at the RANS–LES interface.

Contents

6 Figures

(22 pages in total)

List of figures

This page is intentionally left blank.

1 Introduction

An important issue in methods similar to the Detached Eddy Simulation (DES) method of Spalart *et al.* (Ref. 13) such as X-LES is the development of free shear layers starting from turbulent boundary layers. Even though free shear layers are intrinsically unstable, computational results may show stable shear layers of lengths that seem unphysical (see, e.g., Spalart (Ref. 12)). In our experience, this behaviour is not necessarily caused by excessive levels of dissipation as it is also found when the shear layer is fully captured in LES mode using fine grids and high-order numerical schemes (and even if no subgrid-scale model is used). Instead, it appears that the unstable modes of the shear layer are simply not triggered because the computations are void of any disturbances, either physical or numerical. In this paper, the subgrid-scale model employed in X-LES is extended with a stochastic term, destabilizing the shear layer and leading to rapid development of fully 3D turbulence.

In DES-type methods, the turbulent boundary layers upstream of a free shear layer are typically in RANS mode and therefore do not contain any resolved turbulence. As a consequence, the development of turbulence in the shear layer will start from the intrinsic instability of the shear layer and will not be forced by turbulence coming from the boundary layers. This resembles the situation when the upstream boundary layers are laminar. In that case, however, the distance over which the initial, essentially 2D, Kelvin–Helmholtz instabilities develop into fully 3D turbulence may be very long (of the order of hundreds of initial displacement thicknesses or more, see Huang & Ho (Ref. 4)).

One possible approach to resolve this issue is by adding LES content at the RANS–LES interface, forcing the development of 3D turbulence in the shear layer. This is feasible in a zonal RANS–LES approach. In X-LES and similar DES-type methods, however, the RANS–LES interface is dynamic, which complicates adding LES content. Therefore, an alternative method to speed-up the shear-layer development is considered. This method consists of adding a stochastic term to the subgrid-scale (SGS) model. Stochastic SGS models have been used in the literature to model backscatter, seen as a random forcing of the resolved scales through non-linear interactions with the subgrid scales (e.g., Leith (Ref. 9), Schumann (Ref. 11)). Here, the main goal is not to model backscatter, but to see if a stochastic SGS model can act as a disturbance to trigger 3D instabilities in the shear layer.

2 Modelling

2.1 The X-LES method

The X-LES formulation (Ref. 7) is a particular DES method (Ref. 13) that consists of a composition of a RANS k–ω turbulence model and a k-equation SGS model. Both models use the Boussinesq hypothesis to model the Reynolds or subgrid-scale stress tensor, which depends on the eddy-viscosity coefficient ν_t. Furthermore, both models are based on the equation for the modelled turbulent kinetic energy k, which depends on its dissipation rate ε. Both the eddy viscosity and the dissipation rate are modelled using the turbulent kinetic energy as velocity scale together with a length scale l_t,

$$\nu_t = l_t \sqrt{k} \quad \text{and} \quad \varepsilon = \beta_k \frac{k^{3/2}}{l_t}, \tag{1}$$

where l_t is defined as a combination of the RANS length scale $l = \sqrt{k}/\omega$ and the SGS filter width Δ,

$$l_t = \min\{l, C_1 \Delta\}, \tag{2}$$

with $C_1 = 0.05$. The RANS k–ω model is completed by an equation for the specific dissipation rate ω. The X-LES method will be in LES mode if $C_1\Delta < l$. Note that in that case the SGS model is completely independent of ω.

2.2 Stochastic subgrid-scale model

In the standard X-LES method (and in most other DES-type methods), the SGS stress tensor is modelled using the Boussinesq hypothesis, which essentially means that the effect of the subgrid-scale turbulent fluctuations on the resolved scales is modelled as a diffusion process. In the representation of this diffusion process, however, the 'randomness' of the subgrid-scale fluctuations is lost. An alternative representation of diffusion, based on an analogy with the random-walk process, is given by the following stochastic PDE:

$$\phi(x, t + \delta t) = \phi(x, t) + \delta t\, \nu\, \xi_i \xi_j \frac{\partial^2 \phi}{\partial x_i \partial x_j}, \tag{3}$$

where the vector components ξ_i (the random-walk direction) are independent stochastic variables with standard normal distribution N(0, 1), so that $\mathrm{E}(\xi_i) = 0$ and $\mathrm{E}(\xi_i \xi_j) = \delta_{ij}$. Note that the expectation of this equation is the standard diffusion equation.

To incorporate this stochastic diffusion model in the SGS model, the cross terms are dropped and a single stochastic variable $\xi = \mathrm{N}(0, 1)$ is used for all three vector components. The stochastic

diffusion model then reduces to the standard diffusion equation with a stochastic diffusion coefficient $\nu^* = \xi^2\nu$. In the same way, the stochastic variable can be included in the expression for the SGS eddy viscosity:

$$\nu_t = \xi^2 C_1 \Delta \sqrt{k}. \tag{4}$$

At each time step, a new value of ξ is drawn for every grid cell.

The stochastic SGS eddy viscosity should only be used when the X-LES method is in LES mode, not when it is in RANS mode. One option is to multiply $C_1\Delta$ with ξ^2 in the expression for l_t (equation (2)). This, however, would make the switching between RANS and LES modes as well as the dissipation rate ε dependent on the stochastic variable. Instead, the eddy viscosity is set explicitly as

$$\nu_t = \begin{cases} k/\omega & \text{if } l \le C_1\Delta\,, \\ \xi^2 C_1 \Delta \sqrt{k} & \text{if } l > C_1\Delta\,, \end{cases} \tag{5}$$

while the expressions for l_t and ε are left unaltered.

2.3 Zonal RANS–LES method

As the stochastic SGS model is effective throughout the complete LES zone, it may have other effects besides triggering the shear-layer instabilities. Therefore, as a reference, also a different approach to destabilizing the shear layer is considered. A zonal RANS–LES method is used, setting the boundary layers explicitly to RANS and the shear layers explicitly to LES. The same turbulence models as in the X-LES method are used, i.e., the RANS k–ω turbulence model and the k-equation SGS model. At the RANS–LES interface, LES content is added to the solution in the LES zone. This added LES content may destabilize the shear layer, while the original SGS model is maintained in the complete LES zone. Developing methods for introducing LES content is currently an active research area, for example, using precursor data (Ref. 10) or synthetic turbulence (Refs. 1, 5). Here, a simple model for the LES content is chosen, based on white noise and introducing isotropic resolved stresses. Although such an approach requires a significant distance to develop realistic turbulence, it is considered sufficient for our present purpose (i.e., reference method for destabilizing the shear layer).

To introduce the LES content, the following flux is added to the LES momentum equation at the interface:

$$\rho(\bar{u}_i u'_j + u'_i \bar{u}_j + u'_i u'_j + \tau^r_{ij}) n_j, \tag{6}$$

with the ρ density, $\bar{u}_i$ the time-averaged velocity vector, u_i' the added resolved turbulent velocity fluctuations, τ_{ij}^r the added resolved turbulence, and n_i the unit vector normal to the interface. This flux was derived by subtracting the RANS equations from the LES equations. For the time-averaged velocity, the instantaneous RANS velocity is used. The turbulent velocity fluctuations are computed as

$$u_i' = \sqrt{\tfrac{2}{3}k^r}\xi_i, \tag{7}$$

where k^r is the desired resolved turbulent kinetic energy. Again, the vector components ξ_i are independent stochastic variables with standard normal distribution N(0, 1). This approach introduces isotropic resolved stresses, given by

$$\tau_{ij}^r = -\overline{u_i' u_j'} = -\tfrac{2}{3}k^r\delta_{ij}. \tag{8}$$

Alternatively, a non-isotropic stress tensor can be introduced by including the Choleski decomposition of the resolved stress tensor in the model for u_i' (see Batten et al. (Ref. 1)). Note that the expectation or time average of the additional momentum flux equals zero, so that no net momentum source is created.

The desired resolved turbulent kinetic energy (k^r) is equal to the modelled turbulent kinetic energy in the RANS zone (k^R) minus the time-averaged SGS turbulent kinetic energy (k^s),

$$k^r = k^R - k^s, \tag{9}$$

where for k^R the solution of the k-equation at the RANS side of the interface is used. The value of k^s is determined by comparing the RANS and SGS models of the dissipation rate,

$$\varepsilon^R = \frac{\beta_k (k^R)^{3/2}}{l} \quad \text{and} \quad \varepsilon^s = \frac{\beta_k (k^s)^{3/2}}{C_1 \Delta}. \tag{10}$$

Because the dissipation of resolved stresses can be neglected (viscous dissipation taking place at the Kolmogorov scales), the two modelled dissipation rates should be equal. This gives the following relation between k^s and k^R:

$$k^s = \alpha k^R \quad \text{with} \quad \alpha = \left(\frac{C_1 \Delta}{l}\right)^{2/3}, \tag{11}$$

so that finally

$$k^r = (1 - \alpha) k^R. \tag{12}$$

In regions where $\alpha > 1$, the value of k^r is set to zero.

3 Results

3.1 Plane free shear layer

As a basic test case for investigating the stability issue, the experiment of Delville (Ref. 2) for a plane free shear layer is considered. The free shear layer starts from the trailing edge of a flat plate with free-stream velocities $u_1 = 41.54\,\mathrm{m/s}$ and $u_2 = 22.40\,\mathrm{m/s}$ at the different sides of the flat plate. At the trailing edge, the turbulent boundary layers are fully developed with the momentum and displacement thicknesses equal to $\theta_1 = 1.0\,\mathrm{mm}$ and $\delta_1^* = 1.4\,\mathrm{mm}$ at the high-speed side and $\theta_2 = 0.73\,\mathrm{mm}$ and $\delta_2^* = 1.0\,\mathrm{mm}$ at the low-speed side. The θ-based Reynolds number at the high-speed side is $Re_{\theta_1} = 2900$ at the trailing edge. The shear layer develops in a $0.3\,\mathrm{m} \times 0.3\,\mathrm{m}$ square test section of length 1.2 m. A self-similar flow with fully developed turbulence is reached well within the test section.

A computational domain is used with a width of 0.15 m (z-direction) and a height of 0.3 m (y-direction). To capture the correct boundary-layer profiles at the trailing edge, the flat plate has a length of 0.5 m on the high-speed side and 0.3 m on the low-speed side and fine-tuning has been done by varying the transition locations. The grid is stretched in the y-direction to capture the boundary layers with approximately $y^+ = 1$ for the first grid cell. A computational 'test section' is defined with a length of 1 m after the trailing edge and with a uniform grid in the x- and z-directions, followed by a buffer zone of 1 m length with a stretched grid in x-direction.

Two grid levels are used, G1 and G2, with 1.29 and 10.3 million grid cells. Grid G2 has 96 cells in z-direction and 640 cells in x-direction in the computational test section, giving a mesh size $h = 1.5625\,\mathrm{mm}$ in both directions (similar to Tenaud (Ref. 14)). The filter width Δ is set equal to this mesh size. For grid G2, a dimensionless time step of $\delta t^+ = u_1 \delta t / L = 0.0016$ is used (with the length of the test section, $L = 1\,\mathrm{m}$, as reference length), giving a CFL number $u_1 \delta t / h = 1$. For grid G1 the mesh sizes, the time step, and the filter width are all doubled compared to G2.

Computations are performed with a high-order finite-volume method that has low numerical dissipation and dispersion and that preserves the skew-symmetry of convection (Ref. 6). This method was designed for the LES regions of hybrid RANS–LES computations and was shown to significantly improve the grid convergence with a fixed filter width (Ref. 8).

First, standard X-LES computations are performed on grid G1. The computations are started from the solution of a steady X-LES computation, which was not converged and therefore contains 3D perturbations of the shear layer. Initially, instabilities in the shear layer are visible shortly after the trailing edge (Fig. 1a), but as the computation continues, the shear layer stabilizes with

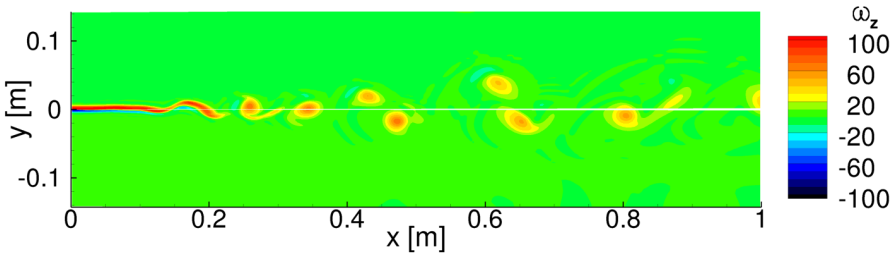

(a) After 500 time steps (time $t^+ = 1.6$)

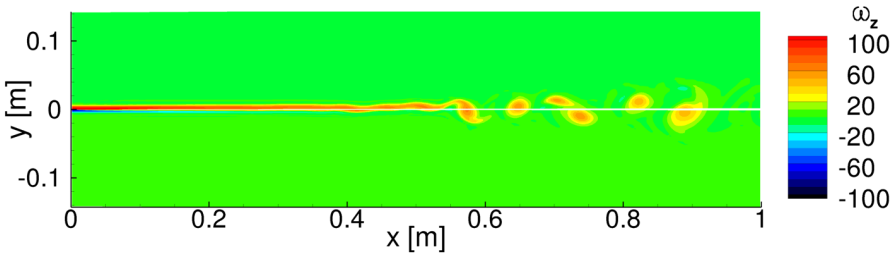

(b) After 3500 time steps (time $t^+ = 11.2$)

Fig. 1 Instantaneous contours of vorticity (y-component) for standard X-LES computation of plane shear layer on grid G1 (1.29 million cells).

the first visible instabilities shifting down to a location of approximately 0.4 m after the trailing edge (Fig. 1b). Moreover, even though the solution originally contains 3D disturbances, it becomes quickly two-dimensional (Fig. 2a). The solution essentially displays the behaviour of an initially laminar shear layer: growth of a 2D Kelvin–Helmholtz instability followed by vortex pairing. For such a shear layer, fully developed 3D turbulence is only reached after a distance of at least $10\lambda_0/R$ with λ_0 the initial instability wavelength and $R = (u_1 - u_2)/(u_1 + u_2)$ (Ref. 4). In this case, $\lambda_0 \approx 60$ mm and $R = 0.3$, giving a distance of at least 2 m.

A possible cause for slow shear-layer development is an excessive level of dissipation. The presented computation, however, uses a high-order finite-volume method with low numerical dissipation on a grid with high resolution in all directions. It has been verified that the shear layer is fully captured in LES mode. Switching off the SGS model completely in the shear layer or continuing the computation on the finer grid G2 makes no essential difference. Therefore, it is concluded that, in this case, the slow development is not caused by high dissipation. Instead, the lack of any kind of disturbance in the computation, either physical or numerical, is perceived as a possible cause.

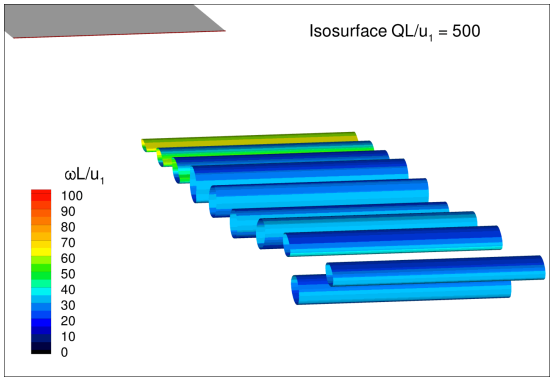

(a) Standard X-LES on grid G1 (time $t^+ = 9.6$)

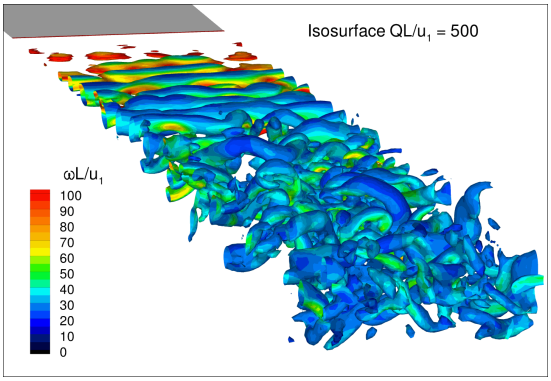

(b) X-LES with stochastic SGS model on grid G1 (time $t^+ = 9.6$)

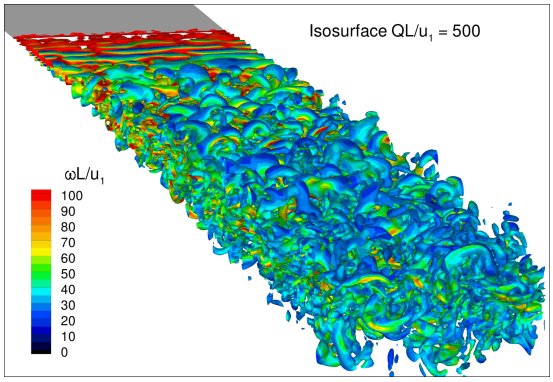

(c) X-LES with stochastic SGS model on grid G2 (time $t^+ = 4.8$)

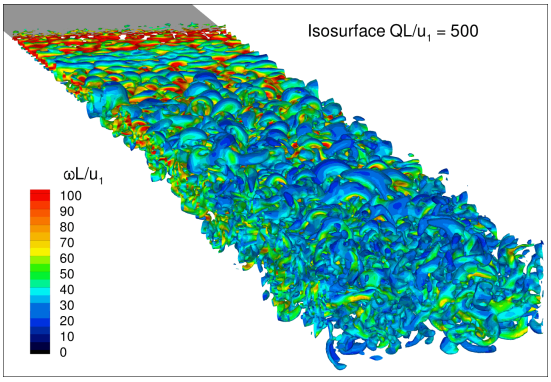

(d) Zonal RANS-LES on grid G2 (time $t^+ = 1.6$)

Fig. 2 Instantaneous isosurfaces of $Q = \omega^2 - S^2$, coloured with vorticity magnitude ω, for X-LES and zonal RANS–LES computations of plane shear layer (S is magnitude of rate-of-strain).

Using the stochastic SGS model in X-LES results in a dramatic improvement for the plane free shear layer. The initial, spanwise vortices appear much closer to the trailing edge and already show 3D disturbances (Fig. 2b). The flow then rapidly develops fully 3D turbulence. Continuing the stochastic X-LES computations on grid G2 (Fig. 2c), the shear layer develops even quicker and finer turbulent structures are captured. As a reference, zonal RANS–LES computations are also performed on grid G2 (Fig. 2d). The initial, spanwise vortices show stronger 3D disturbance than stochastic X-LES, but the subsequent development of the shear layer appears similar, showing similar fine-scale structures.

The mean velocity and resolved stresses are computed by averaging in time (over at least 2000 times steps) and in the spanwise direction. Self-similar solutions are obtained for stochastic X-LES and for zonal RANS–LES within the test section. Fig. 3 compares these self-similar solutions at three stations towards the end of the test section with the experimental results. The similarity coordinate is given by $\eta = (y - y_{1/2})/\theta$, with $y_{1/2}$ the location where $u^+ = (u - u_2)/(u_1 - u_2) = \frac{1}{2}$ and θ the shear-layer momentum thickness. The profiles of the mean velocity and the resolved shear stresses of the computations are close to each other and to the experiment. For the resolved normal stresses, the stochastic X-LES and zonal RANS–LES results on grid G2 are close to each other and show only a small difference with the experiment, whereas the stochastic X-LES results on grid G1 deviate more strongly.

The main difference between the computations and the experiment is seen in the growth of the shear layer in terms of the momentum thickness (Fig. 4). The experiment shows a linear growth over a large part of the test section, which is consistent with a self-similar solution. The computations on grid G2 initially show a larger growth rate ($\mathrm{d}\theta/\mathrm{d}x$) but tend towards the same rate as the experiment near the end of the test section. Again, the strongest difference with the experiment is found for the stochastic X-LES results on grid G1 with a significantly larger spreading rate over the entire test section.

Note that the present methods do not aim to resolve a significant part of the turbulence coming from the boundary layers. Therefore, the initial development of the shear layer differs from the experiment, which results in different initial momentum thicknesses. The best one can expect is a rapid development towards the same similarity solution with a similar spreading rate.

3.2 Supersonic base flow

Finally, as a less academic application, the supersonic base flow of a cylindrical afterbody is considered (experiment of Herrin & Dutton (Ref. 3), free-stream Mach number $M_\infty = 2.46$,

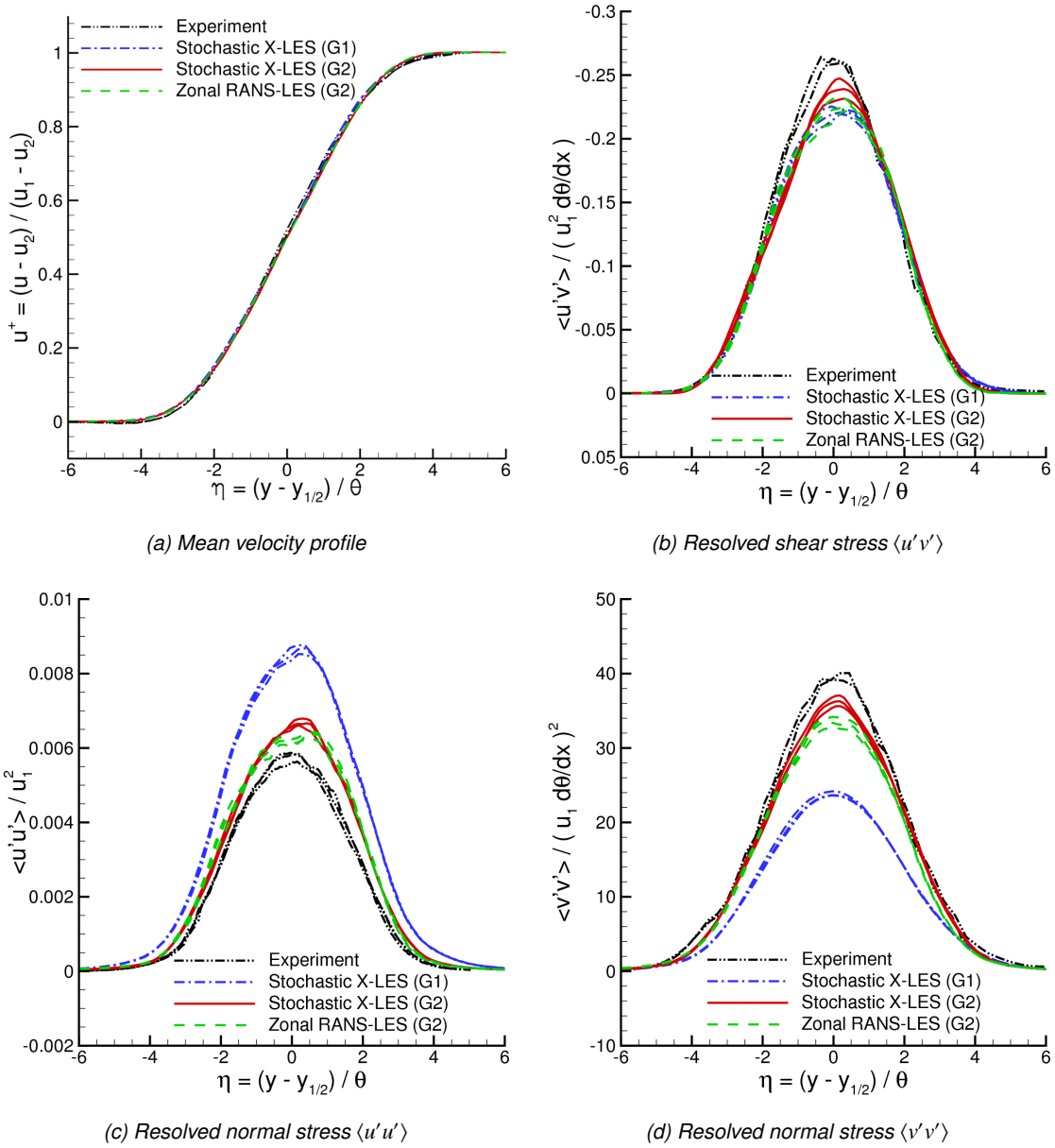

(a) Mean velocity profile

(b) Resolved shear stress $\langle u'v' \rangle$

(c) Resolved normal stress $\langle u'u' \rangle$

(d) Resolved normal stress $\langle v'v' \rangle$

Fig. 3 Self-similar solution for X-LES and zonal RANS–LES computations of plane shear layer compared to experiment of Delville (Ref. 2).

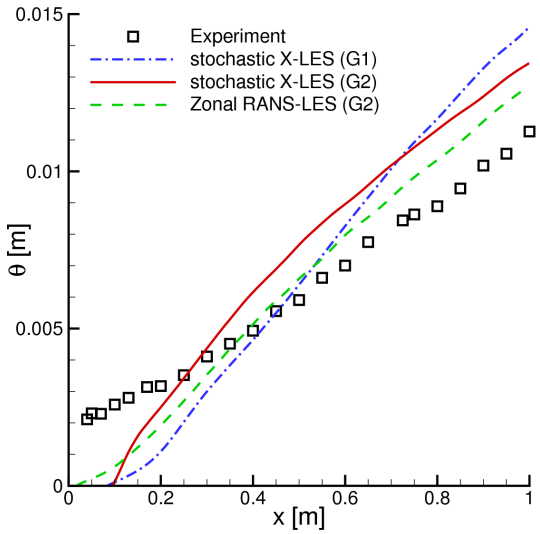

Fig. 4 Momentum thickness for X-LES and zonal RANS–LES computations of plane shear layer compared to experiment of Delville (Ref. 2).

Reynolds number based on diameter $Re_D = 3.3 \cdot 10^6$). A grid of 4.4 million cells, with a typical mesh size $h = 0.015D$, and a time step of $\delta t^+ = u_\infty \delta t/D = 0.0033$ are used. In this case, the shear-layer stability issue is less severe, because unstable modes may be triggered by the resolved turbulence that is convected in the wake of the base towards the shear layer onset.

In a standard X-LES computation, the shear layer develops too slowly, leading to an overprediction of the size of the wake. In fact, as the computation continues, the level of resolved turbulent kinetic energy in the shear layer keeps dropping, its peak keeps shifting down stream, and the size of the wake keeps growing. Even the final solution (after 19,500 time steps, i.e.,. a time interval $t^+ = 64.4$) seems not to have settled yet (and therefore has been averaged over a relatively small time interval of 6,000 time steps). With the stochastic X-LES method, the computation does settle well within 17,000 time steps (and has been averaged over the last 10,000 time steps). As a result, the stochastic method predicts higher levels of resolved turbulent kinetic energy (Fig. 5a) that compare better to the experiment (Fig. 5b) and a smaller size of the wake, also closer to the experiment (Fig. 6).

Despite these improvements, a clear overprediction of the size of the wake, compared to the experiment, remains. The initial development of the shear layer still appears to be too slow. As the grid in the initial shear layer is relatively coarse, locally refining the grid may possibly improve the results.

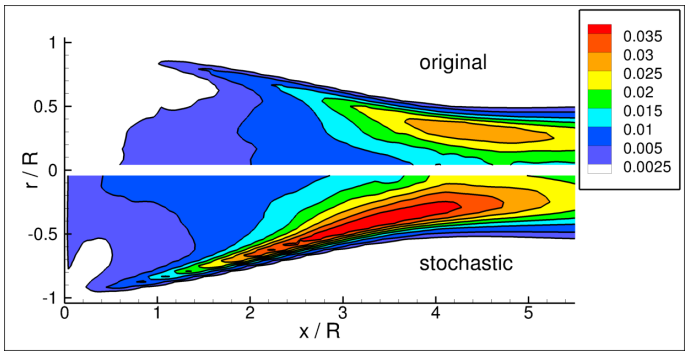

(a) Stochastic and standard X-LES

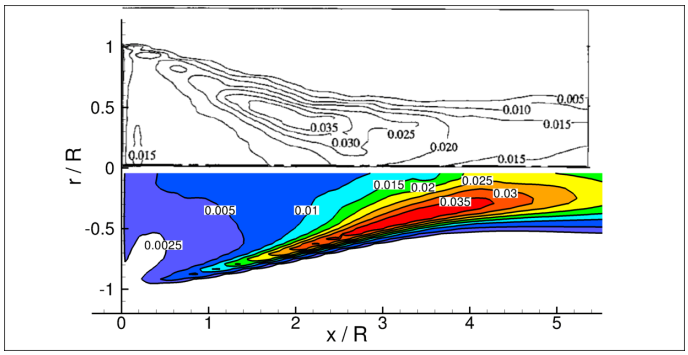

(b) Stochastic X-LES and experiment

Fig. 5 Resolved turbulent kinetic energy for X-LES computation of supersonic base flow of a cylindrical afterbody compared to experiment of Herrin & Dutton (Ref. 3).

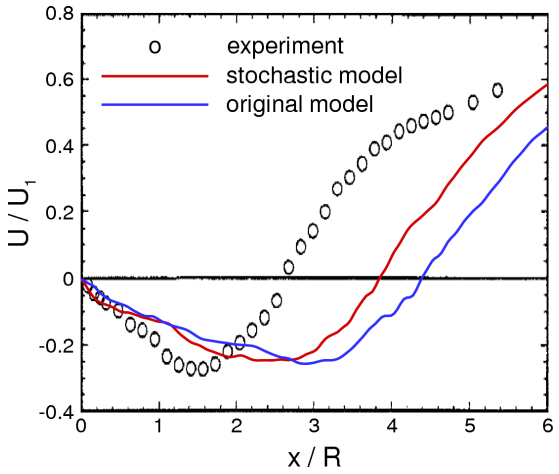

Fig. 6 Mean axial velocity component along wake axis for X-LES computation of supersonic base flow of a cylindrical afterbody compared to experiment of Herrin & Dutton (Ref. 3).

4 Conclusion

Turbulent free shear layers as computed in DES-type methods such as X-LES may be stable over a length that is inconsistent with experiments. Here, it has been shown that this is not necessarily due to excessive levels of dissipation that stabilize the shear layer, but that it can also occur for computations on fine grids using high-order numerical methods. Apparently, the computations are void of any disturbances that can induce the rapid growth of shear-layer instabilities. Instead, the shear layer develops only slowly, similar to an initially laminar shear layer. With the introduction of a stochastic term in the subgrid-scale model, the shear layers in X-LES computations are destabilized and realistic, full 3D turbulence develops more rapidly.

Acknowledgement

This work has been performed within the NLR programme ‘Kennis als Vermogen, Platformtechnology and Flight Physics’.

References

1. P. Batten, U. Goldberg, and S. Chakravarthy. Interfacing statistical turbulence closures with large-eddy simulation. *AIAA Journal*, 42(3):485–492, March 2004.
2. J. Delville. *La décomposition orthogonal aux valeurs propres et l'analyse de l'organisation tridimensionnelle de écoulements turbulents cisaillés libres*. PhD thesis, Université de Poitiers, 1995.
3. J. L. Herrin and J. C. Dutton. Supersonic base flow experiments in the near wake of a cylindrical afterbody. *AIAA Journal*, 32(1):77–83, January 1994.
4. L.-S. Huang and C.-M. Ho. Small-scale transition in a plane mixing layer. *Journal of Fluid Mechanics*, 210:475–500, 1990.
5. N. Jarrin, J.-C. Uribe, R. Prosser, and D. Laurence. Synthetic inflow boundary conditions for wall bounded flows. In S. H. Peng and W. Haase, editors, *Advances in Hybrid RANS–LES Modelling*, volume 97 of *Notes on Numerical Fluid Mechanics and Multidisciplinary Design*, pages 77–86. Springer, 2008.
6. J. C. Kok. A high-order low-dispersion symmetry-preserving finite-volume method for compressible flow on curvilinear grids. *Journal of Computational Physics*, 228:6811–6832, 2009. (NLR-TP-2008-775).
7. J. C. Kok, H. S. Dol, B. Oskam, and H. van der Ven. Extra-large eddy simulation of massively separated flows. In *42nd AIAA Aerospace Sciences Meeting*, Reno, NV, 5–8 January 2004. AIAA paper 2004-264.
8. J. C. Kok, B. I. Soemarwoto, and H. van der Ven. X-LES simulations using a high-order finite-volume scheme. In S. H. Peng and W. Haase, editors, *Advances in Hybrid RANS–LES Modelling*, volume 97 of *Notes on Numerical Fluid Mechanics and Multidisciplinary Design*, pages 87–96. Springer, 2008.
9. C. E. Leith. Stochastic backscatter in a subgrid-scale model: Plane shear mixing layer. *Phyisics of Fluids A*, 2(3):297–299, March 1990.
10. J. U. Schlüter, H. Pitsch, and P. Moin. Large eddy simulation inflow conditions for coupling with Reynolds-averaged flow solvers. *AIAA Journal*, 42(3):478–484, March 2004.
11. U. Schumann. Stochastic backscatter of turbulence energy and scalar variance by random subgrid-scale fluxes. *Proc. R. Soc. Lond. A*, 451:293–318, 1995.
12. P. R. Spalart. Detached-eddy simulation. *Annual Review of Fluid Mechanics*, 41:181–202, January 2009.
13. P. R. Spalart, W.-H. Jou, M. Strelets, and S. R. Allmaras. Comments on the feasibility of LES for wings, and on a hybrid RANS/LES approach. In C. Liu and Z. Liu, editors, *Ad-*

vances in DNS/LES. Greyden Press, 1997. Proc. 1st AFOSR Int. Conf. on DNS/LES, 1997, Ruston (LA), USA.

14. C. Tenaud, S. Pellerin, A. Dulieu, and L. Ta Phuoc. Large eddy simulations of a spatially developing incompressible 3D mixing layer using the $v - \omega$ formulation. *Computers & Fluids*, 34:67–96, 2005.